v. 3, n. 5, 2023

Journal of
Engineering
Research

EFFICIENT PHENOL DEGRADATION BY TIO_2 NANOPARTICLES DOPED WITH NON-EXPENSIVE METALS

Daiane Kessler Fischer
Laboratory of Catalysis and Nanomaterials, School of Chemistry and Food, Federal University of Rio Grande - FURG
Santo Antônio da Patrulha, RS, Brazil

Karina Rodrigues de Fraga
Laboratory of Catalysis and Nanomaterials, School of Chemistry and Food, Federal University of Rio Grande - FURG
Santo Antônio da Patrulha, RS, Brazil

Carla Weber Scheeren
Laboratory of Catalysis and Nanomaterials, School of Chemistry and Food, Federal University of Rio Grande - FURG
Santo Antônio da Patrulha, RS, Brazil

Abstract: In this work, TiO_2 nanoparticles were synthesized and doped using non-expensive metals Cu^{2+} and Fe^{3+} by the sol–gel method. The 1% Cu^{2+}-doped TiO_2 NPs and 1% Fe^{3+}-doped TiO_2 NPs photocatalysts were been characterized by Scanning electron microscopy and dispersive X-ray spectroscopy (SEM/EDX), Transmission electron microscopy (TEM), Brunauer-Emmett-Teller analysis (BET), Fourier transform infrared spectroscopy (FTIR) and X ray diffraction (XRD) to determine its morphological, textural and structural characteristics. XRD analysis confirmed the presence of two crystalline phases, anatase (majority) and rutile. SEM micrographs showed spherical particles of the TiO_2 and compact layers for 1% Cu^{2+} and 1% Fe^{3+}-doped TiO_2 NPs. EDX analysis confirmed only the presence of Ti, O, Fe and Cu. BET analysis exhibited that mesoporous materials were generated, with pore diameter between 12-16 nm and similar values for surface area (55-63 m^2/g). The TEM images exhibited spherical shape nanoparticles with mean diameter of 20-22 nm. The Cu^{2+} and Fe^{3+}-doped TiO_2 NPs photocatalysts, were investigated on phenol degradation under UV/Visible irradiation and quantified by HPLC-FLD. The catalytic activity was investigated in different concentrations (0.5; 1; 5 and 10%) metal-TiO_2 NPs. The best catalytic activity occurred at phenol photodegradation by Cu^{2+} and Fe^{3+}-doped TiO_2 NPs atomic ratio 1.0 percent. The photocatalysts 1% Cu^{2+}-doped TiO_2 NPs and 1% Fe^{3+}-doped TiO_2 NPs exhibited high catalytic activity (99.9%) in phenol degradation.

Keywords: Copper and Iron ions- doped TiO_2 NPs, Sol-gel method, Characterization, Phenol photodegradation.

INTRODUCTION

The phenolic compounds represent an important class of polluting organic molecules presents in wastewater. Pesticides, chemicals, petrochemicals, paints, textiles, biotechnological industries and food processing, generate these compounds (Balasundram et al. 2006).

These compounds are highly toxic and their presence preventing microorganisms activity in biological wastewater reducing the bio degradation of the other components (Raza et al.; 2019; Guerra et al. 2001). Several technologies exhibit phenol degradation in effluents (Singh et al. 2018). As example, we can cite biological treatment, activated carbon adsorption and advanced oxidative processes (AOP) (Dixit et al. 2020; Mukhrjee et al. 2017; Suzuki et al. 2015; Vosoughi et al. 2017; Kanakaraju et al. 2018; Shailesh et al. 2018). Photocatalysis stands out among the techniques of advanced oxidative processes (AOP). This consists of activating a semiconductor by sunlight or artificial light. One of the main semiconductors used is TiO_2, which demonstrates efficiency in the photodegradation of organic compounds (Shailesh, et al. 2018; Ibhadon and Fitzpatrick 2013; Li, et al. 2014).

The TiO_2 has shown to be the most suitable catalyst for environmental applications, considering its biological and chemical inertness, strong oxidizing power, non–toxicity, insolubility and stability against chemical corrosion (Vosoughi et al. 2018; Kanakaraju et al. 2018; Ibhadon and Fitzpatrick 2013). This semiconductor when at the nanoscale has a pronounced effect on its photocatalytic properties, due to its larger surface area, exhibiting a high percentage of its constitutive atoms on the particle surface (Ibhadon and Fitzpatrick 2013). The metal ions addiction to TiO_2, provide a good control of the main particle size to produce nanocatalysts (Li et al. 2014). The doping of TiO_2 by transition metal cations

is an efficient strategy to reduce electron–hole recombination rate and increase photocatalytic efficiency (Vosoughi et al. 2017).

Noble metals such as Au are most studied; but other metals such as palladium, copper and iron have been reported to be useful for photocatalytic reactions. The sol–gel method is widely used to prepare metal ion doped TiO_2 due to its facility to control pore structures and concentration (Yoon et al. 2005). When TiO_2 undergoes UV-vis irradiation with energy equal to or greater than *semiconductor band gap energy,* the valence band electrons are excited for the conduction band generating an electron pair. The formed gap has an extremely oxidizing potential. The water adsorbed on the surface of TiO_2 interacts with the gap hydroxyl radicals ($^{\cdot}OH$), capable of reducing organic matter to CO_2, water and mineral ions (Fujishima et al. 2000; Chao et al. 2019; Suh et al. 2019; Nahar et al. 2006).

In this work, we conducted the study of the photocatalytic properties of TiO_2 nanoparticles doped with non-expensive metals Fe^{3+} and Cu^{2+}. The synthesized photocatalysts were applied in phenol degradation, thus evaluating the effect of doping and photocatalytic efficiency. The photocatalysts showed higher photocatalytic activity and were been characterized by scanning electron microscopy (SEM), dispersive energy spectroscopy (EDS), transmission electron microscopy (TEM), surface area analysis (BET), Fourier transform infrared spectroscopy (FTIR) and X ray diffraction (XRD).

EXPERIMENTAL

SYNTHESIS OF FE^{3+} AND CU^{2+} -DOPED TIO_2 NPS:

The Fe^{3+} and Cu^{2+}-doped TiO_2 NPs synthesis occurred by mixing of ethanol (25 mL) and Titanium tetraisopropoxide (TTIP) (2.5 mL) under stirring during 10 minutes in a bottle (Moradi et al. 2016). For pH adjusting, sulfuric acid solution (0,125 mL) was added dropwise to the solution, stirring was continued at long of this time (30 minutes). Then 25 mL double distilled water and 121 mL absolute propanol were stirred and added dropwise to the solution. For doped TiO_2, $Fe(SO_4)_3.5H_2O$ or $Cu(SO_4).5H_2O$ were added to this solution in different atomic ratio and stirring continued for 90 minutes. For gel formation and exit of alcohol, the formed sol was stirred at room temperature for 24 h; after that, the gel was dried under vacuum at 90°C for about 12 h and then calcined at 600 °C for 1 h (Moradi et al. 2016).

PHENOL DEGRADATION

Phenol photodegradation was performed using a photo reactor 250 mL composed of a stirring system, digital thermometer and a UV light source (consisting of a low-pressure mercury vapor lamp of 150 W, from which the bulb was removed). In the experimental photocatalytic degradation of up mentioned concentrations of phenol (10 mg/L) at pH 3 and using different atomic ratio (0.5; 1; 5 and 10%) metal-doped TiO_2 NPs under UV irradiation (380 nm) was investigated. The irradiation time was 180 minutes and aliquots of solution were collected from the reactor after intervals 15 minutes. In the experiments the magnetic stirrer was employed to keep the suspensions uniform. Samples were centrifuged (6000 r/min for 5 min) and filtered to separate Fe^{3+} or Cu^{2+}-doped TiO_2 particles. The aliquots were analyzed by HPLC-FLD of Agilent brand, model 1260. The injections of the samples were performed according to the parameters established, with a flow of 1.5 mL/min, running time of 35 minutes, post-run of 10 minutes, injection volume 20 µL,

Lichrospher RP column 18 and 5 µm, 250 x 4 mm and guard column C18, 4 x 3 mm. The results were quantified based on the peak area, using chemstation *software* (Wu et al. 2015).

CHARACTERIZATION

FOURIER TRANSFORM INFRARED SPECTROPHOTOMETER (FTIR)

The samples were analyzed in the infrared region with readings from 4000 to 400 cm^{-1} using the Spectrophotometer of the brand Shimadzu, model IR PRESTIGE-21. The samples were prepared in solid form in potassium bromide (KBr) tablets and the generated data were treated with the aid of origin pro 8.0 software (Suwanchawalit et al. 2010).

SCANNING ELECTRON MICROSCOPE (SEM), DISPERSIVE ENERGY SPECTROSCOPY (EDX)

The SEM and EDX analyses were performed in a Scanning Electron Microscope, in high and low vacuum mode, Jeol, JSM - 6610LV, operating at 20 kV. To perform the analysis, the samples were deposited in stubs and metallized with gold using the Denton Vacuum Desk V equipment.

TRANSMISSION ELECTRON MICROSCOPE (TEM)

For the TEM analyses, samples were prepared by dispersing of the TiO_2 NPs in isopropanol and deposited in a copper grid, coated with carbon film. The counts were performed with the aid of the Image J *software*.

X RAY DIFFRACTION (XRD)

X ray Diffraction analyses were performed using an X-ray diffometer with a chamber for cryogenic temperatures, Bruker, D8 Advance with the following parameters: Voltage: 40kV, Current: 40mA, copper tube and wavelength (λ): 1.5418Å. The generated data processed with the help of origin pro 8.0 *software*.

BRUNAUER, EMMETT, TELLER (BET) ANALYSIS

Surface Area analyses were performed on the Gemini VII 2390A - Micromeritics Surface Area Analyzer. The sample was thermally pretreated at 400°C for 2 hours under nitrogen flow.

RESULTS AND DISCUSSION

The $Cu^{2+}$and Fe^{3+}- doped TiO_2 NPs photocatalysts were been synthesized using different atomic ratio by sol-gel method. The process involves hydrolysis/condensation, gelification/polymerization steps, aging and drying to form the product (Hench and West 1990). The formation of the colloidal solution, sun stage, was observed through the formation of a whitish and milky solution and the gel step by a white and viscous precipitate. The gel was subjected to drying to remove the interstitial liquid solvent, and a progressive shrinkage, tension and fragmentation of the material were observed. At the end of the drying and maceration process, a powder of different stains was obtained, which are directly related to the metal precursor/TiO_2 NPs atomic ratio used in the synthesis process (Figure 1).

Figure 1. Photocatalysts: A) NPsTiO_2 B) 0.5% Cu^{2+}-doped TiO_2 NPs, C) 1% Cu^{2+}-doped TiO_2 NPs D) 5% Cu^{2+}-doped TiO_2 NPs, D) 0.5% Fe^{3+}-doped TiO_2 NPs, E) 1% Fe^{3+}-doped TiO_2 NPs F) 5% Fe^{3+}-doped TiO_2 NPs, G) 10% Fe^{3+}-doped TiO_2 NPs.

The photocatalysts were been characterized by different analysis. The photocatalysts 1% Cu^{2+} and 1% Fe^{3+}-doped TiO_2 NPs were first characterized by XRD (Figure 2). The XRD analysis showed a composition of the anatase (55%) and rutile (45%) phases for the 1% Cu^{2+}-doped TiO_2 NPs photocatalyst and rutile (30%), anatase (70%) for the 1% Fe^{3+}-doped TiO_2 NPs photocatalyst. This presence of phase mix tends to favor the photocatalytic activity of TiO_2, since it minimizes the recombination of photogenerated charges. According to reports exposed in the literature, the presence of phase mix tends to favor the photocatalytic activity of TiO_2, since it minimizes the recombination of photogenerated charges (Machado 2006).

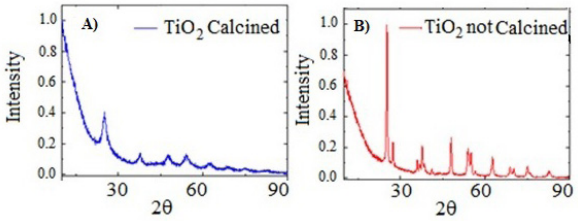

Figure 2. XRD analysis of: A) TiO_2 NPs without calcination and B) TiO_2 NPs calcined.

The photocatalysts TiO_2 NPs, 1% Cu^{2+}-doped TiO_2 NPs and 1% Fe^{3+}-doped TiO_2 NPs calcined and the TiO_2 NPs without calcination process were characterized by XRD. The crystalline phases of the photocatalysts and the effect of calcination on the crystalline structure were analyzed. The analyses of the TiO_2 NPs, 1% Cu^{2+}- doped TiO_2 NPs and 1% Fe^{3+}-doped TiO_2 NPs photocatalysts calcined showed crystalline planes and intensities according to their crystalline phase, and can be characterized by the values of the 2θ angles and the Miller indexes (h k l), characteristic of each phase of TiO_2.

In Figure 3, in the diphrates obtained it is possible to observe the planes in 25.35°, 38.16°, 48.06°, 55.03° and 62.22° corresponding to the reflections of the crystalline planes, (101), (112), (200), (211) and (204), respectively, characteristic of the anatase phase. The compounds also presented planes of the rutile crystalline phase at 27.68°, 36.22°, 41.65° and 54.26° that correspond to the reflections of the crystalline planes (110), (101), (111) and (211), respectively (Ling et al. 2015). In all photocatalysts analyzed, the anatase and rutile phases were observed, and the presence of the broquite crystalline phase was not observed (Tong et al. 2008; Hossain et al. 2021). It is possible to verify that the TiO_2 NPs without calcination does not display the characteristic planes of the crystalline phases of TiO_2, so an amorphous material was obtained. The calcination is a fundamental role in the formation of the crystalline phases of TiO_2, and temperature is a determining factor in the composition of the crystalline phases of the material.

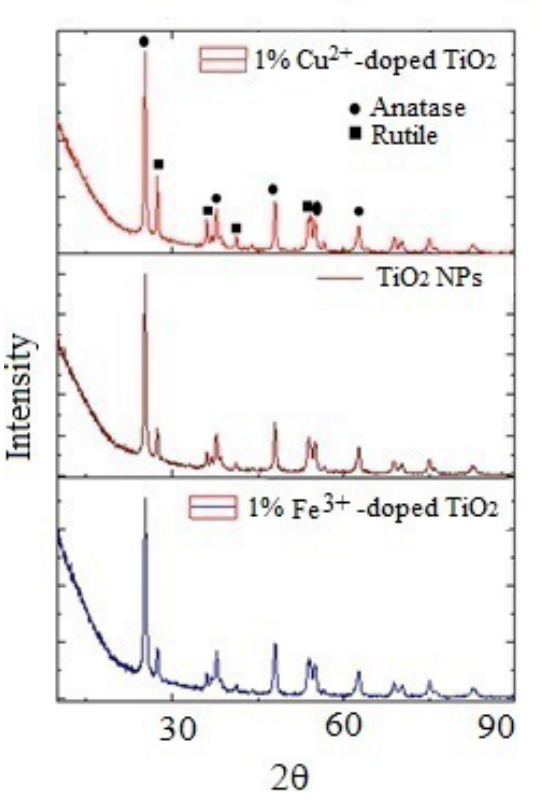

Figure 3. XRD analysis: A) 1% Cu^{2+}- doped TiO_2 NPs, B) TiO_2 NPs and C) 1% Fe^{3+}- doped TiO_2 NPs.

The results obtained through XRD analysis are in accordance with the results described in the literature for TiO_2. In one study were reported (TONG et al. 2008) analysis of XRD characteristic of the anatase phase. The values found were 25.24°, 36.98°, 48.02° and 62.74°, corresponding to the diffraction plans (101), (004), (200) and (204). (Ling et al. 2015) In another study, diffraction plans of the anatase phase (101), (004), (103), (112), (200), (105), (211) and (204) were found, in addition to the plans of the rutile phase (110), (101) and (310). (Braga et al. 2015) A review of XRD analysis peaks from the International Committee Database for powder diffraction patterns for the crystalline anatase, rutile and broquite phase was presented. For the anatase phase, the patterns were described 25.304° (101), 33.454° (110), 38.566° (112), 48.037° (200) and 55.061° (211). For the rutile phase, the expected diffraction patterns are 27.475° (110), 36.154° (101), 41,326° (111) and 54.442° (211) and for the broquita phase the plan 31,146° (211) was reported in the TiO_2 NPs.

The FTIR spectrum (Figure 4) obtained for the photocatalysts TiO_2 NPs, 1% Cu^{2+}-doped TiO_2 NPs and 1% Fe^{3+}-doped TiO_2 NPs, exhibited a band at 1630 cm^{-1} associated with angular deformation of the water adsorbed on the surface of the photocatalysts, HOH, v_{HOH} (Suwanchawalit and Wongnawa 2010). The band obtained in the low energy region between 400 and 900 cm^{-1}, more precisely at 750 cm^{-1}, is attributed to overlaps of vibration bands v_{Ti-O} and $\delta_{Ti-O-Ti}$ characteristics of TiO_2 obtained by the sol-gel method. The vibration band at 3300 cm^{-1} is related to Ti-OH, v_{Ti-OH} (Suwanchawalit C, Wongnawa S, 2010).

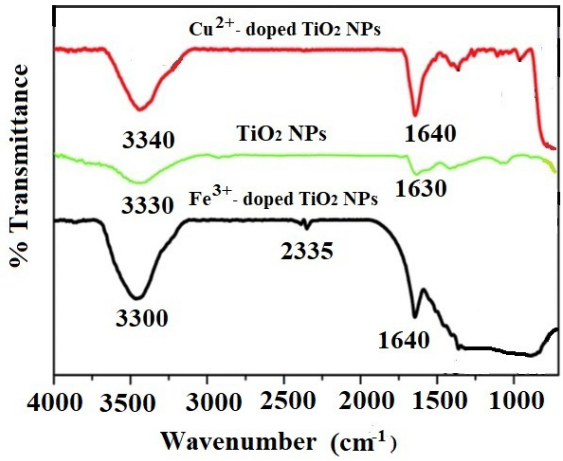

Figure 4. FTIR spectrum of the TiO_2 NPs, 1% Cu^{2+}- doped TiO_2 NPS and 1% Fe^{3+}-doped TiO_2 NPs.

For the TiO_2 NPs, 1% Cu^{2+}-doped TiO_2 NPs and 1% Fe^{3+}-doped TiO_2 NPs photocatalysts, the same infrared spectrum pattern was observed, confirming that for all cases, TiO_2 was insorbed with water adsorbed the structure. Another band that was observed in the FTIR spectrum is the band in the region of 2335 cm^{-1} related to Ti-O connection of TiO This band has already been observed according to the literature (ANWAR et al. 2015).

The SEM micrographs of the TiO_2 NPs, 1% Cu^{2+}-doped TiO_2 NPs and 1% Fe^{3+}-doped TiO_2 NPs photocatalysts are exposed in Figure 5.

The SEM micrographs obtained for the TiO_2 NPs (Figure 6A) exhibit spherical particles formation. The photocatalysts 1% Cu^{2+}-doped TiO_2 NPs (Figure 6B) and 1% Fe^{3+}-doped TiO_2 NPs (Figure 6C) showed layered and compact materials. The layered and compact surface structure presented by photocatalysts have been previously described in the literature (Moradi et al. 2016; Haque et al. 2017). The EDX analysis were performed together with the SEM analysis for the materials TiO_2 NPs, 1% Cu^{2+}-doped TiO_2 NPs and 1% Fe^{3+}-doped TiO_2

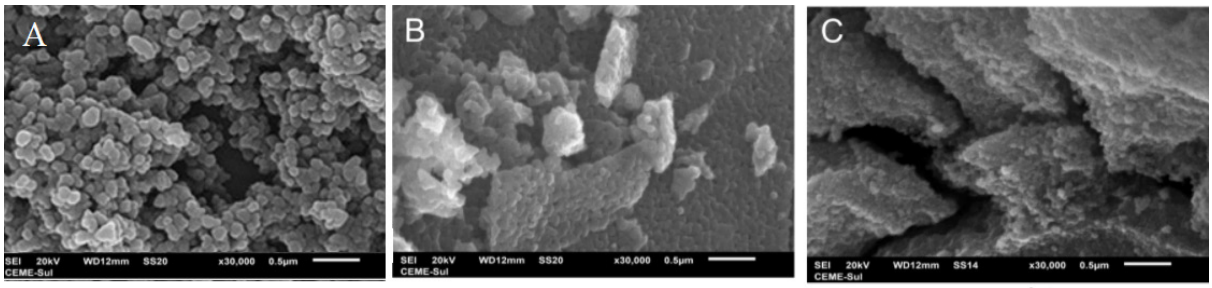

Figure 5. SEM micrographs obtained for samples: A) TiO_2 NPs, B) 1% Cu^{2+}-doped TiO_2 NPs and C) 1% Fe^{3+}-doped TiO_2 NPS

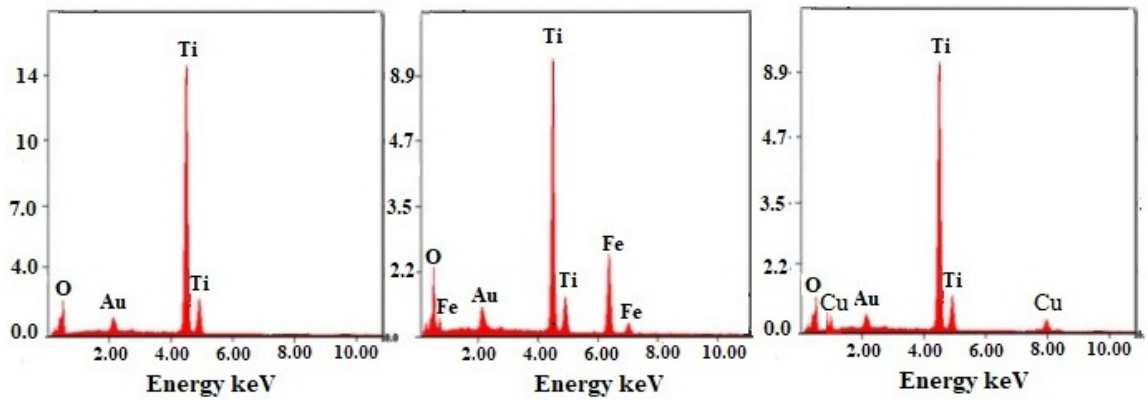

Figure 6. Dispersive energy spectra: A) TiO_2 NPs, B) 1% Fe^{3+}-doped TiO_2 NPs and C) 1% Cu^{2+}-doped TiO_2 NPs.

NPs. The energy dispersion spectra obtained for the described samples can be exposed in Figure 7.

Through the bonding energies present it was possible to prove that only Ti and O elements were detected it the TiO_2 NPs photocatalyst. For the photocatalysts 1% Fe^{3+}- doped TiO_2 NPs, only Fe, Ti, O elements were detected and for 1% Cu^{2+}- doped TiO_2 NPs only Cu, Ti, O elements were observed. The qualitative quantification of the chemical elements present in the described samples is been described in Table 2.

The photocatalysts were prepared using isopropanol dispersion and a drop of the dispersion obtained was deposited in a carbon-covered copper grid for TEM analysis. The micrographs obtained by TEM are exposed in Figure 7.

In the Table 3 are showed the average diameters obtained for TiO_2 NPs, 1 % Fe^{3+}-doped TiO_2 NPs and 1% Cu^{2+}-doped TiO_2 NPs obtained by TEM analysis. Through the micrographs (Figure 8), it is possible to verify that the TiO_2 NPs, as well as, for the 1% Fe^{3+}-doped TiO_2 NPs and 1% Cu^{2+}-doped TiO_2 NPs have manometer diameter (18-22 nm), spherical shape and are preferably agglomerated. The agglomeration observed for the metal-doped materials may be related to the nanometer diameter of the particles that constitute the fine powder of the materials studied.

The average diameters of NPsTiO_2 obtained in this study are very similar to those reported in the literature. As an example, we can mention the synthesis of NPsTiO_2 doped with iron that exhibited diameters in

Material	Element Chemical	%m/m
TiO_2 NPs	Ti	54.9
	O	36.31
1% Fe^{3+}-doped TiO_2 NPs	Ti	46.73
	O	38.09
	Fe	0.85
1% Cu^{2+}-doped TiO_2 NPs	Ti	50.48
	O	37.87
	Cu	0.69

Table 2: Percentage mass/mass of chemical elements present in TiO_2 NPs, 1% Fe^{3+}- doped TiO_2 NPs and 1% Cu^{2+}- doped TiO_2 NPs analyzed by SEM/EDX.

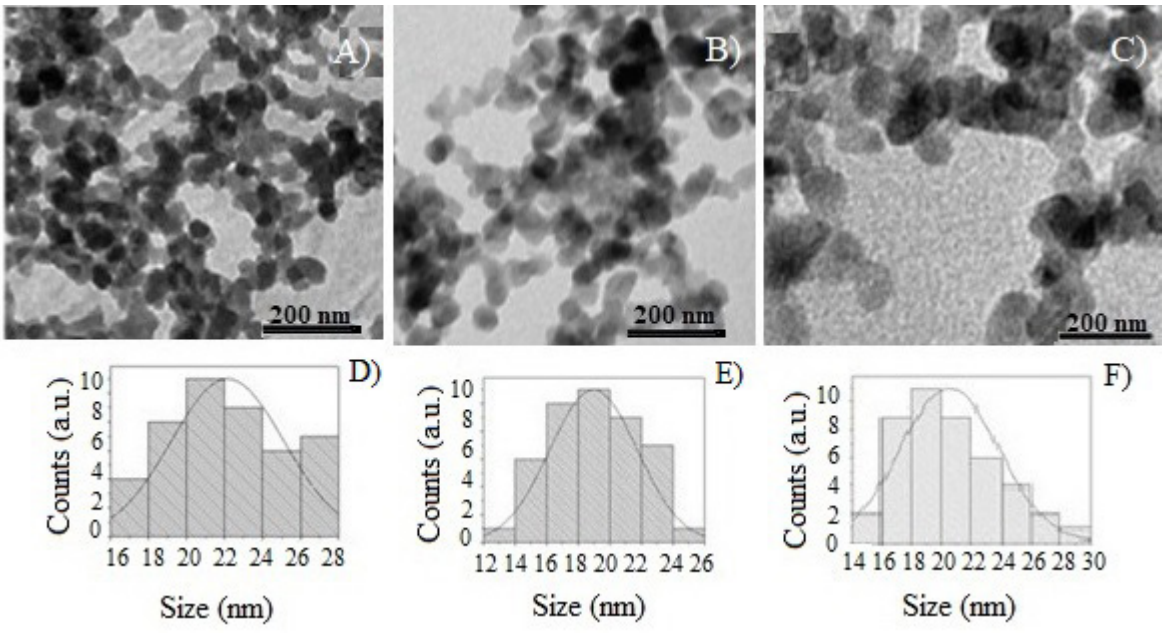

Figure 7. TEM analysis of the photocatalysts: A) TiO_2 NPs B) 1% Cu^{2+}-doped TiO_2 NPs C) 1% Fe^{3+}- doped TiO_2 NPs D) Histogram of diameter distribution for TiO_2 NPs E) 1% Cu^{2+}-doped TiO_2 NPs F) Histogram of diameter distribution for 1% Fe^{3+}- doped TiO_2 NPs .

Material	Average particle diameter (nm)
NPsTiO_2	21.8 ± 2.96
1% Fe^{3+}-doped TiO_2 NPs	18.9 ± 2.78
1% Cu^{2+}-doped TiO_2 NPs	20.2 ± 3.2

Table 3. Average diameter and standard deviation of particles obtained for TiO_2 NPs, 1% Fe^{3+}-doped TiO_2 NPs and 1% Cu^{2+}-doped TiO_2 NPs analyzed by TEM.

the range of 9-20 nm (George et al. 2011). In another study, the synthesis of NPsTiO_2 formed particles with diameters ranging in the range between 9-23 nm (LING et al. 2015). In another example, TiO_2 NPs doped with iron was performed at different calcination temperatures. In the calcination at 400°C were obtained particles of average diameter from 6 to 11 nm and only anatase phase were observed. In calcination at 600°C was observed change from anatase to rutile phase, with anatase phase in predominance and average diameter from 22 to 30 nm, at calcination at 800°C only the rutile phase was observed with an average diameter of 50 to 100nm (Nasralla et al. 2013).

The Scherrer equation is widely applied to determine the average diameters of the particles in a manometer scale. In Table 4, based in the results it is possible to verify that the diameter obtained of the TiO_2 NPs by XRD are smaller than those obtained by TEM. The difference observed between XRD and TEM analysis indicates that the observed particles (Figure 8) may not be a single crystalline, but clusters of isolated crystallites with a smaller particle diameter than that observed in the TEM image (Tong et al. 2008).

TEM analysis of the 1% Fe^{3+}-doped TiO_2 NPs and 1% Cu^{2+}-doped TiO_2 NPs also presented smaller diameter when compared to XRD analysis. This result shows that the doping of the material with metal ions causes a decrease in particle diameter. This fact occurs in relation to the incorporation of metal ions into the crystalline structure of TiO_2, generating a deformation due to the different atomic sizes, as an example, the Fe^{3+} (0.69Ů) and Ti^{4+} (0.745Ů) ions. The deformation presented in the crystal line-up results in the restriction of the growth of Fe^{3+}-TiO_2 crystals, decreasing the diameter of the TiO_2 crystal (Tong et al. 2008).

Photocatalysts	XRD diameter (nm)
TiO_2 NPs	14.4
1% Fe^{3+}-doped TiO_2 NPs	11.2
1% Cu^{2+}-doped TiO_2 NPs	14.9

Table 4. XRD analysis of the photocatalysts, TiO_2 NPs, 1% Fe^{3+}-doped TiO_2 NPs and 1% Cu^{2+}-doped TiO_2 NPs

Table 5 shows the percentages calculated for the crystalline anatase and rutile phases for the samples: TiO_2 NPs, 1% Cu^{2+}-doped TiO_2 NPs and 1% Fe^{3+}-doped TiO_2 NPs.

Photocatalyst	Anatase phase (%)	Rutile phase (%)
TiO_2 NPs	64	35
1% Cu^{2+}- doped TiO_2 NPs	55	45
1% Fe^{3+}-doped TiO_2 NPs	70	30

Table 5. Composition of the crystalline phase of photocatalysts estimated from XRD analysis

After copper doping, the crystalline phase of TiO_2 NPs presented a higher proportion of the rutile crystalline phase than the other materials studied. This result may be related to the use of doping with cations that present a lower number of valence electrons than the number of valence electrons of the matrix cation, thus generating anion vacancies. In other words, when TiO_2 is doped with Cu^{2+} cations, these tend to diffuse through the structure and replace Ti^{4+} ions, moving from the O-Ti-O to Cu-O connection, thus leading to the formation of oxygen vacancies (Anwar and Mulyadi 2015; Yang et al. 2015). The presence of oxygen vacancies favors the transition from anatase to rutile phase, because the presence of these vacancies decreases the network deformation energy that must be overcome for the rearrangement of anatase to rutile octahedrons. The unit cell of the anatase phase is composed of 24 Ti-O

connections. For the formation of the rutile phase it is necessary to break 7 bonds of the anatase phase to occur the rearrangement. With the presence of oxygen vacancies in the crystalline network of TiO_2, the number of Ti-O connections that need to be broken become smaller, thus facilitating the transition from the anatase to rutile phase in materials doped with Cu^{2+} ions.

The surface area, pore volume and pore size were determined by BET analysis for the TiO_2 NPs, 1% Fe^{3+}-doped TiO_2 NPs and 1% Cu^{2+}-doped TiO_2 NPs photocatalysts and the results are shown in Table 6.

Material	Surface area (m^2/g)	Pore volume ($^3cm/g$)	Pore diameter (nm)
TiO_2 NPs	58.9	0.24	16.2
1% Fe^{3+} -doped TiO_2 NPs	63.6	0.20	12.5
1% Cu^{2+} -doped TiO_2 NPs	55.0	0.21	15.2

Table 6. Surface area, Pore volume and pore diameter by BET analysis of the TiO_2 NPs, 1% Fe^{3+}-doped TiO_2 NPs and 1% Cu^{2+}-doped TiO_2 NPs photocatalysts.

BET analysis provided information about surface area, pore volume and pore diameter values for the different photocatalysts studied. For the TiO_2 NPs sample, the value of surface area was 58.9, for 1% Fe^{3+}/NPs TiO_2 was 63.6 and for 1% Cu^{2+}/NPs TiO_2 was 55.0 (Wang et al. 2011; Sun et al. 2012; Hinojosa-Reyes et al. 2017). The results described that copper doping caused minimal reduction in the surface area of the doped TiO_2 NPs (1% Cu^{2+} when compared to the pure TiO_2 NPs). The addition of metal ions to TiO_2 NPs did not significantly alter the surface area or pore volume of the materials studied. This fact is related to the effects of calcination temperature on the surface area and pore diameter, which causes decreases in the surface area. The photocatalysts symthesized were calcined at constant temperature (600°C), this fact justifies the approximate values of surface area, volume and pore size. Based on the values obtained the synthesized materials can be classified as mesoporous, considering that they presented pore size from 12-16 nm.

Comparing the obtained results by SEM and BET analysis, it can be observed through the SEM micrographs exhibited surface structure different between TiO_2 NPs and doped photocatalysts, TiO_2 NPs showed spherical particles and the 1% Cu^{2+}-doped TiO_2 NPs and 1% Fe^{3+}-doped TiO_2 NPs exhibited a compact layers surface. However, BET analysis exhibited that surface area values are similar for the all photocatalysts analyzed, 58.9 m^2/g (TiO_2 NPs), 63.6 m^2/g (1% Fe^{3+}-doped TiO_2 NPs) and 55 m^2/g (1% Cu^{2+}-doped TiO_2 NPs). These results show that the organization of the surface structure is different but the properties are similar.

The $Cu^{2+}$and Fe^{3+}- doped TiO_2 NPs photocatalysts in different metal atomic ratio (0.5 %; 1 %; 5 % and 10 %) were first applied in phenol photodegradation for evaluation of the catalytic activity. The results obtained in phenol photodegradation showed that the more active photocatalysts were 1% Cu^{2+}-doped TiO_2 NPs (99.9 %) and 1 % Fe^{3+}-doped TiO_2 NPs (96.6%) (Figure 8). The result is related due to oxidation potential of Fe^{3+}species being (-0.77 V) and Cu^{2+} species (-0.15 V). Thus, the Cu^{2+} species has a greater tendency to be oxidized by dissolved oxygen, thus initiating the photocatalysis cycle and with a greater recombination between the photogenerated electron and Cu^{2+} ions, leaving the gap in valence band more time available for the generation of OH radicals (Kashif and Ouyang 2009). The other photocatalysts studied; 0.5% Cu^{2+}-doped

TiO_2 NPs, 5% Cu^{2+}-doped TiO_2 NPs, 0.5% Fe^{3+}-doped TiO_2 NPs, 5% Fe^{3+}-doped TiO_2 NPs and 10% Fe^{3+}-doped TiO_2 NPs do not showed phenol photodegradation greater than 60%.

In catalytic processes, an important factor is the proportion of catalyst/substrate. The Figure 8 shows the influence of the catalyst concentration on phenol photodegradation. The experiments exhibited that with the increase in concentration of catalyst from 0.5 to 1% (m/m), the photodegradation of phenol increases (43% to 96%). This result is due to the fact that the increase in the number of Fe^{3+}-doped TiO_2 NPs or Cu^{2+}-doped TiO_2 NPs increase the number of photons absorbed, the active sites and the number of the phenol molecule adsorbed. However, there was not a considerable increase in phenol photodegradation when catalyst concentration was increased from 1% to 5% or 10%. This is attributed to catalyst agglomeration when in high concentration. The opacity and screening effect of excess Fe^{3+}-doped TiO_2 or Cu^{2+}-doped TiO_2 NPs act as surface layer on the surface, reducing light penetration, decreasing the active surface area, reduction in photon absorption and consequently decreasing the catalytic activity. Therefore, the best concentration of Fe^{3+}-doped TiO_2 NPs or Cu^{2+}-doped TiO_2 NPs determined as 1% (m/m). The 1% Cu^{2+} and 1% Fe^{3+}-doped TiO_2 NPs synthesized using the sol-gel method at 90 °C and calcined at 600 °C during 1 h generated the photocatalytic materials.

CONCLUSION

The use of the sol-gel method in the synthesis of the photocatalysts under UV/Vis irradiation, using non-expensive metals Fe^{3+} and Cu^{2+}- doped TiO_2 NPs proved to be effective in generating highly active catalysts in phenol degradation (99.9 %).

The active TiO_2 NPs, 1% Cu^{2+} and 1% Fe^{3+}-doped TiO_2 NPs photocatalysts were been characterized by Scanning electron microscopy and Dispersive X-ray spectroscopy (SEM/EDX), Transmission electron microscopy (TEM), Brunauer-Emmett-Teller analysis (BET), Fourier transform infrared spectroscopy (FTIR) and X-ray diffraction (XRD) for the determination of morphology, texture and structural characteristics. The FTIR analysis showed the presence of characteristic bands to the formation of the connections ν_{Ti-O} and $\delta_{Ti-O-Ti}$ in the photocatalysts analyzed, confirming the formation of the TiO_2 NPs.

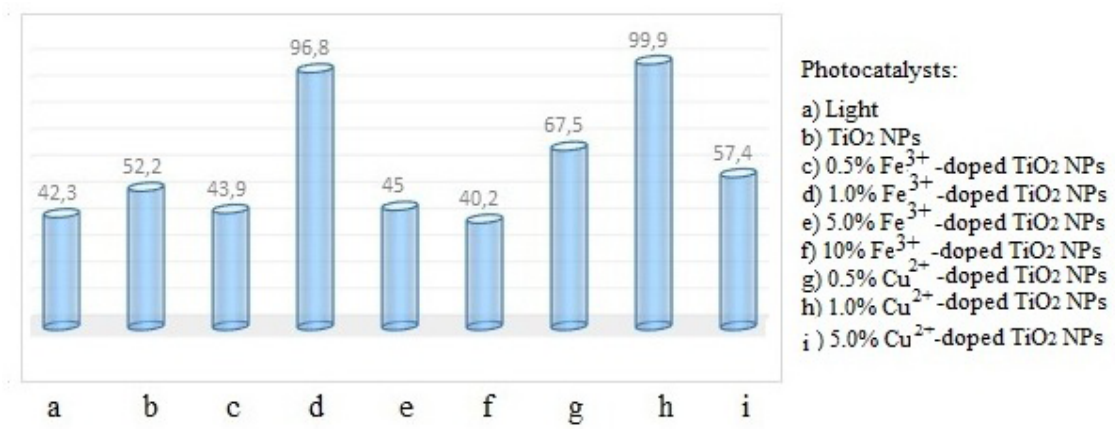

Figure 8. Phenol photodegradation: a) UV light, b) NPsTiO_2, c) 0.5% Cu^{2+}, d) 1% Cu^{2+}, e) 5% Cu^{2+}, f) 0.5% Fe^{3+}, g) 1% Fe^{3+}, h) 5% Fe^{3+} and i) 10% Fe^{3+}.

BET analysis showed that similar surface area (55-63 m^2/g) and pore diameter 12-16 nm. XRD analysis confirmed the presence of two crystalline phases of TiO_2, anatase (majority) and rutile, with particle diameter 11-14 nm. SEM micrographs showed spherical particles formation for TiO_2 NPs and a compact layers for 1% Cu^{2+} and 1% Fe^{3+}-doped TiO_2 NPs. EDX analysis confirmed only the presence of Ti, O, Fe and Cu in the analyzed photocatalysts. The TEM images exhibited spherical shape, for all photocatalysts with average diameter of 18-20 nm and agglomerated preferentially. The smaller particle diameter observed by XRD occurs in relation to the incorporation of metal ions into the crystalline structure of TiO_2, causing decrease in diameter.

REFERENCES

Anwar DI, Mulyadi D (2015) Synthesis of Fe-TiO_2 Composite as a Photocatalyst for Degradation of Methylene Blue. Procedia Chemistry 17: 49–54.

Chao J, Duan D, Xing S, Zhao Y, Zhang X, Gao S, Li X, Fan Q, Yang J (2019) Visible-light-driven photocatalytic properties and electronic structures of nickel sulfide nanoflowers. Solid State Sciences 43: 59 – 62.

Fujishima A, Rao TN, Tryk DA (2000) Titanium dioxide photocatalysis. Journal of Photochemistry and Photobiology C: Photochemistry Reviews 1: 1–21.

Haque FZ, Nandanwar R, Singh P (2017) Optik Evaluating photodegradation properties of anatase and rutile TiO_2 nanoparticles for organic compounds. Optik - International Journal for Light and Electron Optics 128: 191–200.

Hench LL, West JK (1990) The Sol-Gel Process. Chem. Rev 90: 33–72

Hinojosa-Reyes M, Camposeco-Solís R, Zanella R, González VR (2017) Hydrogen production by tailoring the brookite and Cu_2O ratio of sol-gel Cu-TiO_2 photocatalysts. Chemosphere 184: 992-1002.

Kashif N, Ouyang F (2009) Parameters effect on heterogeneous photocatalysed degradation of phenol in aqueous dispersion of TiO_2. J Environ. Sci 21: 527–533.

Ling H, Kim K, Liu Z, Shi J, Zhu X, Huang J (2015) Photocatalytic degradation of phenol in water on as prepared and surface modified TiO_2 nanoparticles. Catalysis Today 258: 96 –102.

Moradi H, Hosseini SR, Ghani K, Eshaghi A (2016) Fabrication of Fe-doped TiO_2 nanoparticles and investigation of photocatalytic decolorization of reactive red 198 under visible light irradiation. Ultrasonics Sonochemistry 32: 314 –319.

Mukhrjee S, Kumar S, Mistra AK, Fan M (2007) Removal of phenols from water environment by activated carbon, ash berry and wood charcoal. Chemical Engineering Journal 129: 133–142.

Nahar MS, Hasegawa K, Kagaya S (2006) Photocatalytic degradation of phenol by visible light-responsive iron-doped TiO_2 and spontaneous sedimentation of the TiO_2 particles. Chemosphere 65: 1976 –1982.

Shailesh SS, Kinjal JS, Chiang PC, Lo SL (2018) Catalytic oxidative degradation of phenol using iron oxide promoted sulfonated-ZrO_2 by Advanced Oxidation Processes (AOPs). Journal of the Taiwan Institute of Chemical Engineers 91: 434 – 440.

Suh M, Shen Y, Chan CK, Kim J (2019) Titanium Dioxide-Layered Double Hydroxide Composite Material for Adsorption-Photocatalysis of Water Pollutants. Langmuir 35: 8699 – 8708.

Sun Q, Leng W, Li Z, Xu Y (2012) Effect of surface Fe_2O_3 clusters on the photocatalytic activity of TiO_2 for phenol photodegradation in water. Journal of Hazardous Materials 229-230: 224–232.

Suwanchawalit C, Wongnawa S (2010) Triblock copolymer-templated synthesis of porous TiO_2 and its photocatalytic activity. Journal of Nanoparticle Research 12: 2895–2906.

Tong T, ding J, Tian B, Chen F, He D (2008) Preparation of Fe^{3+}-doped TiO_2 catalysts by controlled hydrolysis of titanium alkoxide and study on their photocatalytic activity for methyl orange degradation. Journal of Hazardous Materials 155: 572–579.

Wang W, Shi Q, Wang Y, Cao J, Liu G, Peng, P (2011) Preparation and characterization of iodine-doped mesoporous TiO_2 by hydrothermal method. Applied Surface Science 257: 3688–3696.

WU S, Brix H, Wallace S, Kuschk, P (2015) Treatment of industrial effluents in constructed wetlands: Challenges, operational strategies and overall performance. Environmental Pollution 201:107–120.

Yang X, Wang S, Sun H, Wang X, Lian J (2015) Preparation and photocatalytic performance of Cu-doped TiO_2 nanoparticles. Transactions of Nonferrous Metals Society of China 25: 504 –509.

Yoon J, Sasaki T, Koshizak N (2005) Dispersion of nanosized noble metals in TiO_2 matrix and their photoelectrode properties. Thin Solid Films 483: 276 – 282.